Mon. Not. R. Astron. Soc. **000**, ??–?? () Printed 1 February 2008 (MN LATEX style file v2.2)

On the morphologies, gas fractions, and star formation rates of small galaxies

Tobias Kaufmann[1] ⋆, Coral Wheeler[1] and James S. Bullock[1]
[1] *Center for Cosmology, Department of Physics and Astronomy, University of California, Irvine, CA 92697*

1 February 2008

ABSTRACT

We use a series of N-body/smoothed particle hydrodynamics simulations and analytic arguments to show that the presence of an effective temperature floor in the interstellar medium at $T_F \sim 10^4$ K naturally explains the tendency for low-mass galaxies to be more spheroidal, more gas rich, and less efficient in converting baryons into stars than larger galaxies. The trend arises because gas pressure support becomes important compared to angular momentum support in small dark matter haloes. We suggest that dwarf galaxies with rotational velocities ~ 40 km s^{-1} do not originate as thin discs, but rather are born as thick, puffy systems. If accreted on to larger haloes, tenuous dwarfs of this kind will be more susceptible to gas loss or tidal transformation than scaled-down versions of larger spirals. For a constant temperature floor, pressure support becomes less important in large haloes, and this produces a tendency for massive isolated galaxies to have thinner discs and more efficient star formation than their less massive counterparts, as observed.

Key words: galaxies: dwarf — galaxies: formation — hydrodynamics — methods: analytical — methods: N-body simulations.

1 INTRODUCTION

It is well established that small galaxies have longer star formation time scales than their larger cousins (e.g. Hunter & Gallagher 1985; van Zee 2001; Kauffmann et al. 2003; Brinchmann et al. 2004; Geha et al. 2006). Dwarf galaxies in the field have higher specific gas fractions (van Zee 2001; Geha et al. 2006) and are morphologically thicker (Dalcanton et al. 2004; Yoachim & Dalcanton 2006) than luminous late-type galaxies. It is common to discuss supernova feedback or radiative feedback as a means to explain these trends (e.g. Dekel & Silk 1986; White & Frenk 1991; Kauffmann et al. 1993; Bullock et al. 2000; Mayer et al. 2001a; Somerville 2002; Dekel & Woo 2003; Kravtsov et al. 2004; Read et al. 2006; Stinson et al. 2006), yet the origin of the observed relations between galaxy properties and their total mass remains open for debate.

In this paper we investigate the simple systematic effect that a gas temperature floor, T_F, has on the star formation efficiencies, gas fractions, and morphologies of galaxies as a function of dark matter halo mass. We show that even a moderate effective temperature floor of $T_F \simeq 10^4$ K, as might arise naturally in the presence of a photo-ionizing background, produces many of the general trends observed. Specifically, pressure support becomes dynamically comparable to angular momentum support in small dark matter haloes, and this causes dwarf galaxies to be systematically puffier and less efficient in converting gas into stars than their larger counterparts.

In what follows we explore a range of values $T_F = (1.5-5)\times 10^4$ K, in order to qualitatively mimic real physical effects that may act to pressurise gas within galaxies. These may include inefficient cooling, heating by an internal or external ultraviolet (UV) background, supernova feedback, turbulent pressure, and cosmic-ray heating, among others. Of course, within a fully realistic galactic interstellar medium (ISM) we expect molecular cooling to produce cold clouds embedded within a warm, pressurised medium (e.g. Mckee & Ostriker 1977; Yepes et al. 1997; Springel & Hernquist 2003; Robertson et al. 2004, 2006) Internal and external heating sources and cooling within the medium should produce a quasi-stable system with an effective temperature that acts to stabilise the galaxy. Unfortunately, the nature of the coupling between various energy sources and the background ISM is poorly understood. Rather than attempt to model these processes, we use T_F as a phenomenological proxy.

Our approach is perhaps most directly relevant to the situation of an ionizing background field that acts to prevent cooling below $\sim 10^4$ K in warm galactic gas. It is well known

⋆ E-mail: tobias.kaufmann@uci.edu

that a UV background can suppress galaxy formation altogether in very small galaxies $\lesssim 30\,\mathrm{km\,s^{-1}}$ (Efstathiou 1992; Thoul & Weinberg 1996; Quinn et al. 1996; Gnedin 2000; Hoeft et al. 2006; Crain et al. 2007) and that this effect can have important implications for the baryonic mass fractions and overall abundance of the smallest galaxies in the universe (e.g. Bullock et al. 2000; Benson et al. 2002; Strigari et al. 2007). In a recent examination, Hoeft et al. (2006) used cosmological simulations with cooling and star formation to show that gas at typical galactic densities will have equilibrium temperatures $\sim (1-3)\times 10^4$ K, and that this temperature is fairly insensitive to the normalisation of the UV flux. This heating strongly suppresses the baryon fraction in haloes smaller than $\sim 20\,\mathrm{km\,s^{-1}}$ in their simulations. Our investigations focus on galaxies that are just above this scale. Specifically, we explore the morphology and star formation efficiency of galaxies that are large enough to accrete warm gas but small enough to be dynamically affected by warm gas pressure.

We note that the effect of a finite temperature floor on dwarf galaxy formation was discussed in a semi-analytic context by Kravtsov et al. (2004), who used the idea to motivate models for low star formation rates in small galaxies; and by Tassis et al. (2006), who used a similar model to investigate the gas fraction and mass-metallicity relationships in dwarf galaxies. Taylor & Webster (2005) studied star formation within equilibrium dwarf galaxies by modeling H_2 cooling within a thermally-balanced $\sim 10^4$ K medium and derived lower limits on self-regulated star formation rates in dwarfs in this context.

In the next section we present an analytic investigation into the importance of baryonic pressure support compared to angular momentum support as a function of virial mass and gas temperature and show that pressure support should become dynamically important in dwarf-galaxy haloes. In §3 we use the N-body/smoothed particle hydrodynamics (SPH) code GASOLINE (Wadsley et al. 2004) to explore galaxy formation with a range of temperature floors and halo masses. We present results on galaxy disc thickness, gas fractions, and star formation rates as a function of galaxy circular velocity. We reserve §4 for discussion and §5 for conclusions.

2 ANALYTICAL EXPECTATIONS

The standard analytic approach for calculating galaxy sizes and morphologies within dark matter haloes assumes that the gas cools to a temperature well below the halo virial temperature, $T_g \ll T_\mathrm{v}$. As a result, the thermal pressure support in the gas is small compared to its angular momentum support. A *thin* disc of star-forming material is the natural outcome (Fall & Efstathiou 1980, Blumenthal et al. 1986). This thin-disc configuration is taken to be the starting point for galaxy formation (and star formation) in most models, including those that model dwarf galaxies (e.g. Kauffmann et al. 1993; Somerville & Primack 1999; Benson et al. 2002; Somerville 2002; Mastropietro et al. 2005; Mayer et al. 2006; Gnedin et al. 2006; Dutton et al. 2007). Here we stress that the thin disc approximation should break down in small haloes where $T_\mathrm{v} \gtrsim T_g \sim 10^4$ K. In these cases, the pressure support radius becomes comparable to the angular momentum support radius and we expect a thick morphology. What follows is a simple analytic investigation aimed at quantifying the halo mass scale of relevance. A more rigorous numerical approach is given in the next section.

Consider dark matter haloes of mass M_v with virial radii defined[1] such that $R_\mathrm{v} \simeq 113\,\mathrm{kpc}\,(M_\mathrm{v}/10^{11}M_\odot)^{1/3}$. We assume that halo density profiles are well approximated by the NFW fit (Navarro, Frenk, & White 1996):

$$\rho(x) = \frac{\rho_s}{x(x+1)^2}\,, \qquad (1)$$

where $x \equiv r/r_s$ and the scale radius, r_s, is determined from the halo concentration parameter $c_\mathrm{v} \equiv R_\mathrm{v}/r_s$. We adopt the relation $c_\mathrm{v} = 10\,(M_\mathrm{v}/10^{11}\,M_\odot)^{-0.086}$, which is appropriate for a $\sigma_8 = 0.75$ ΛCDM cosmology (Bullock et al. 2001a; Macciò et al. 2007). Given M_v and c_v, the circular velocity curve, $V_c^2(r) = GM(r)/r$, is determined by the integrated mass profile. For our adopted relation, the circular velocity peaks at a maximum value $V_\mathrm{max} \simeq 71\mathrm{km\,s^{-1}}(M_\mathrm{v}/10^{11}\,M_\odot)^{0.3}$.

In the standard thin-disc scenario, the gas obtains specific angular momentum that is similar to that of the dark matter, which is often characterised by a dimensionless spin parameter (Peebles 1969) defined as $\lambda \equiv j\,|E|^{1/2}\,G^{-1}\,M_\mathrm{v}^{-3/2}$, where G is Newton's constant and j and E are the specific angular momentum and energy of the halo, respectively. Simulated CDM haloes typically have $\lambda \sim 0.03$ with a 90 % spread between $0.01-0.1$ (e.g. Barnes & Efstathiou 1987; Bullock et al. 2001b; Macciò et al. 2007).

It is straightforward to show that if the gas cools and contracts without angular momentum loss to form a thin, angular momentum supported exponential disc, the disc scale radius is given by (Mo, Mao, & White 1998; hereafter MMW)

$$R_d = \lambda\, R_\mathrm{halo}\, f(c, \lambda, m_d). \qquad (2)$$

Here we assume that the gas falls in from a radius R_halo, defined to be either the virial radius, R_v, or the "cooling radius", R_c, depending on which one is smaller $R_\mathrm{halo} = \min(R_\mathrm{c}, R_\mathrm{v})$. By introducing the cooling radius (White & Frenk 1991) we account for the expectation that hot gas in the outskirts of massive haloes will not have had time to cool since the halo formed. For simplicity, we adopt[2] $R_\mathrm{c} = 129\ \mathrm{kpc}\,V_{120}^{-1/4}$, where V_{120} is the halo maximum circular velocity in units of 120 km s^{-1}. The function f (~ 1) in Equation 2 contains information on the halo profile shape and contraction from baryonic infall, and depends on the initial halo concentration $c \equiv R_\mathrm{halo}/R_\mathrm{s}$ and the disc mass, m_d, in units of the total mass within R_halo.

The three solid lines labelled with λ values in Figure 1 show R_d calculated in the standard thin-disc framework as a function of the (initial) halo V_max value. From top to bottom the lines assume spin parameters $\lambda = 0.1$, 0.03, and 0.01. We have used the fitting formula from MMW $f(c, \lambda, m_d)$ with $m_d = 0.1$. We plot the scale radius as a function of the initial, uncontracted halo V_max in order to facilitate the following comparison.

[1] In our definition, the virial radius contains an average mass density equal to 360 times the matter density of the universe and we adopt $\Omega_m = 1 - \Omega_\Lambda = 0.27$ and with $h = 0.7$.

[2] This approximation was given by Maller & Bullock (2004) for haloes with $V_{120} \gtrsim 1$. Below this scale, the virial radius sets R_halo.

Table 1. Simulated Galaxies

(1) Name	(2) $V_{\rm max}$ [km s^{-1}]	(3) $c_{\rm v}$	(4) $M_{\rm v}$ [10^{10} M$_\odot$]	(5) T_F [10^4 K]	(6) $R_{\rm d}$ [kpc]	(7) $z_{\rm d}$ [kpc]	(8) $V_{2.2}$ [km s^{-1}]
D24	24	14	0.29	1.5	0.37	0.08	37
D24_g	24	14	0.29	1.5	0.35	0.19	35
D28	28	13	0.47	1.5	0.55	0.09	43
D28_g	28	13	0.47	1.5	0.56	0.18	41
D41	41	12	1.6	1.5	0.92	0.10	65
D41_g	41	12	1.6	1.5	1.02	0.16	65
D41_W	41	12	1.6	3.0	0.61	0.13	64
D53	53	11	3.8	1.5	1.32	0.12	84
D53_g	53	11	3.8	1.5	1.34	0.15	84
D53_W	53	11	3.8	3.0	1.05	0.16	82
D53_H	53	11	3.8	5.0	0.77	0.18	84
G74	74	10	11.0	1.5	1.6	0.14†	115
G74_g	74	10	11.0	1.5	2.2*	0.03*	92
G148	148	8	100.	1.5	1.88	0.22†	209
G148_g	148	8	100.	1.5	1.9*	0.02*	217
G168_gHRLS	168	11	115.	3.0	1.94	0.13	213

(1) Names labelled "_g" refer to pure gas runs without star formation whereas names with "_W" and "_H" signify "warm" or "hot" temperature floors and "HRLS" refers to the Milky Way model described in Kaufmann et al. (2007). (2-4) The listed values for $V_{\rm max}$, $c_{\rm v}$ and $M_{\rm v}$ are *initial* halo parameters. (5) T_F is the imposed temperature floor. (6-8) The last three columns list parameters measured in the final galaxy, where R_d and z_d are the exponential scale length and scale height, respectively, and $V_{2.2}$ is the rotational velocity in the gas measured at 2.2 R_d. Disc scale heights marked with (†) are artificially large as a result of numerical heating. Gas disc parameters marked with (∗) are derived from discs which have become Toomre unstable; thin, but spatially irregular.

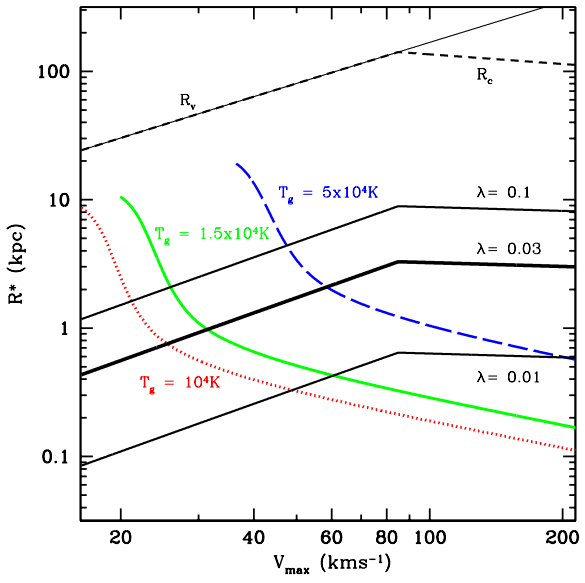

Figure 1. Galaxy radius R^* versus halo $V_{\rm max}$ for various models for galaxy assembly. R^* is defined as the radius that contains 26% of the galaxy mass and is equivalent to the disc scale radius for a thin exponential disc. The solid lines that increase with decreasing halo size show R^* for a pressure-supported isothermal gas with temperature floors as labelled. The straight lines that break at $V_{\rm max} \sim 90\,{\rm km\,s^{-1}}$ show R^* for an angular momentum supported thin disc for three different halo spin parameters as labelled. The break occurs when the infall radius transitions from the virial radius ($R_{\rm v}$) to the cooling radius ($R_{\rm cool}$). Note that the pressure support radius becomes comparable to (and even larger than) the angular momentum support radius in small galaxies.

Consider now the galaxy radius that would result from pressure support in an idealised, spherically symmetric system consisting of a gravitationally sub-dominant gas. Assume that this gas has no angular momentum but reaches a temperature of $T_g = T_{\rm F}$ within an extended NFW halo of virial temperature $T_{\rm v}$. We emphasize that we will calculate the pressure support radius for "cold" gas at $T_g = T_{\rm F}$, the lowest temperature the gas can reach within our assumptions. For this approximate calculation, we neglect baryonic contraction. We will define the virial temperature in analogy with an isothermal gas of temperature T and its associated speed of sound c_s (e.g. Maller & Bullock 2004):

$$T = 10^4 K \left(\frac{c_s}{11.5\,{\rm km\,s^{-1}}}\right)^2 . \quad (3)$$

Specifically, $T_{\rm v}$ is set by using $V_{\rm max}/\sqrt{2}$ for c_s in Equation 3.

The equilibrium gas profile, $\rho_g(r)$, will be set by a competition between the isothermal gas pressure, $P_g = c_g^2 \rho_g$, and the gravitational potential. If we assume that the gravitational force is dominated by the NFW halo potential, the hydrostatic force balance equation

$$\frac{c_g^2}{\rho_g}\frac{d\rho_g}{dr} = \frac{-V^2(r)}{r}, \quad (4)$$

can be rewritten in terms of the dimensionless radial parameter $x = r/r_s$ as

$$\frac{1}{\rho_g}\frac{d\rho_g}{dx} = -\eta\, h(x). \quad (5)$$

Here, $\eta \equiv T_{\rm v}/T_{\rm F}$ parameterises the relative strength of the halo gravity and the thermal pressure of the gas and $h(x) = 9.26x^{-2}\,[\ln(1+x) - x/(1+x)]$. Note that in the limit of large η ($T_{\rm v} \gg T_{\rm F}$), the gas profile will be centrally

concentrated with a large negative derivative, and a negligible pressure-support radius. More generally, solving Equation 5 for ρ_g yields

$$\rho_g(x) = \rho_0 \exp\left[-9.26\,\eta\left(1 - \frac{\ln[1+x]}{x}\right)\right], \quad (6)$$

where the normalisation parameter ρ_0 sets the gas density at $x = 0$. It is clear that in small haloes with $\eta \sim 1$, the gas profile can extend to $x \sim 1$ or $r \sim R_{\rm v}/c \sim 0.1R_{\rm v}$, which is comparable in size to the angular momentum support radius (Eq. 2).

The thick-solid and dotted lines in Figure 1 show a more explicit comparison for various gas floor temperatures: $T_{\rm F} = 1$, 1.5, and 5×10^4 K. We have used Equation 6 to compute the radius R^* that encloses 26% of the pressure-supported galaxy mass as a function of halo $V_{\rm max}$. This radius is analogous to the scale radius for an exponential disc, which contains 26% of the rotationally supported disc mass. While relatively unimportant in large Milky-Way-size haloes ($V_{\rm max} \sim 200\,{\rm km\,s^{-1}}$), we see that pressure support should dominate in shaping galaxy morphologies and gas distributions in small haloes. The expectation is that small galaxies will be intrinsically puffier than large galaxies, even in the absence of environmental influences.

The scale where pressure becomes important compared to rotation will naturally depend on the temperature floor of the gas and on the intrinsic spin. For $T_{\rm F} = 1.5 \times 10^4$ K and $\lambda = 0.03$, we expect the effect to become very important for dwarf-size haloes with $V_{\rm max} \lesssim 35\,{\rm km\,s^{-1}}$. If the temperature floor is high, $T_{\rm F} = 5 \times 10^4$ K, then the effect could be important even in $\sim 100\,{\rm km\,s^{-1}}$ haloes if they have inhabit the low-spin tail of the distribution, $\lambda = 0.01$. If galaxies form with the range of spins expected ($\lambda \sim 0.01 - 0.1$) then we would predict a range of morphologies (from puffy to thin discs) *at fixed* $V_{\rm max}$ as long as the temperature floor is roughly the same from galaxy to galaxy. Though we do not explore galaxy formation in very small halos ($\lesssim 20{\rm km\,s^{-1}}$) in the rest of this paper, it is interesting to note that we expect the morphologies of the smallest objects to be essentially spheroidal, with initially extended gas profiles. The stellar sizes of these objects will likely be much smaller than the gas extent, as high-densities will be required for star formation. This might provide an explanation for why the smallest galaxies (dwarf spheroidals) are always dispersion supported systems.

The simple, spherical, model we have just explored was primarily designed to guide expectations. Stronger results are presented in the next section, where we use 3D hydrodynamical simulations to investigate the effect of a reasonable gas temperature floor on morphologies, gas fractions, and star formation rates in small galaxy haloes.

3 SPH SIMULATIONS

We use the parallel TreeSPH code GASOLINE (Wadsley et al. 2004), which is an extension of the pure N-Body gravity code PKDGRAV developed by Stadel (2001). It includes artificial viscosity using the shear reduced version (Balsara 1995) of the standard Monaghan (1992) implementation. GASOLINE uses a spline kernel with compact support for the softening of the gravitational and SPH quantities. The energy equation is solved using the asymmetric formulation, which is shown to yield very similar results compared to the entropy conserving formulation but conserves energy better (Wadsley et al. 2004). The code includes radiative cooling for a primordial mixture of helium and (atomic) hydrogen. Because of the lack of molecular cooling and metals, the efficiency of our cooling functions drops rapidly below 10^4 K. The lack of molecular cooling is unimportant in our investigation because we enforce temperature floors $T_{\rm F} \geqslant 1.5 \times 10^4$ K.

We investigate runs with and without star formation. The adopted star formation recipe is similar to that described in Katz (1992). Specifically, a gas particle may spawn star particles if i) it is in an over-dense region; ii) it is cool, with $T = T_{\rm F}$; and iii) it has a density greater than a critical threshold, $\rho_g > \rho_{\rm SF}$. In practice, the critical star formation density is the most important parameter. In our primary simulations we use $\rho_{\rm SF} = 2.5 \times 10^6 M_\odot\,{\rm kpc^{-3}}$, but explore a case with $\rho_{\rm SF}$ increased by a factor of 100 in §4. Once a gas particle is eligible for spawning stars, it does so based on a probability distribution function with a star formation efficiency factor c^* that is tuned to match the Kennicutt (1998) Schmidt Law for the Milky Way and M33-size disc described in Kaufmann et al. (2007). The mass of gas particles decreases gradually as they spawn more star particles. After its mass has decreased below 10% of its initial value the gas particle is removed and its mass is re-allocated among the neighboring gas particles. Up to six star particles are then created for each gas particle in the disc. We note that Stinson et al. (2006) have implemented a similar star formation recipe, although they include an allowance for supernova feedback effects using a subgrid, multi-phase model based on blast waves.

3.1 Initial conditions

We simulate 15 isolated systems with masses spanning the scale of dwarf galaxies to large spirals, with *initial* maximum circular velocities that range from $V_{\rm max} = 24$ to $148\,{\rm km\,s^{-1}}$. We also present results from an older simulation of a Milky-Way size galaxy ($V_{\rm max} = 168\,{\rm km\,s^{-1}}$) that was originally discussed in Kaufmann et al. (2007). Haloes are initialised as spherical equilibrium NFW profiles using the methods outlined in Kazantzidis et al. (2004) and we use the mass-concentration relationship discussed in §2 to set the profile parameters. Table 1 lists the specific parameters used in each simulation and provides a reference name for each run.

We initialise a fraction of the total halo mass, $f_{\rm b} = 0.1$, as a hot baryonic component with the same radial distribution as the dark matter and impose a temperature profile such that the gas is initially in hydrostatic equilibrium with an adiabatic equation of state. For all of our fiducial models we choose $\lambda_g = 0.03$ for our gas spin parameter, defined in analogy with the halo spin as $\lambda_g \equiv j_g |E|^{1/2} G^{-1} M_{\rm v}^{-3/2}$. Here, j_g is the average specific angular momentum of the gas, E and $M_{\rm v}$ are the total energy and mass of the *halo*.

The specific angular momentum distribution of the gas is assumed to scale linearly with the cylindrical distance from the angular-momentum axis of the halo, $j \propto r^{1.0}$. This choice is consistent with values found for dark matter haloes within cosmological N-body simulations (Bullock

et al. 2001b). For simplicity, we initialise the dark matter particles with no net angular momentum.

The hot gaseous halo is sampled with $N_g = 10^5$ particles and the dark matter halo with $N_{\rm dm} = 2 \times 10^5$ particles. The force resolution is set to be a fixed fraction of the simulated halo virial radius, $f_{\rm res} = 0.002 R_{\rm v}$. These choices correspond to cases where numerical losses of angular momentum become small (Kaufmann et al. 2007). A detailed description of our initialisation method and results on the evolution of a Milky Way-size galaxy is presented in Kaufmann et al. (2007).

As seen in Table 1, our new simulations sample six halo circular velocity scales spanning those of dwarfs to large spirals. For each $V_{\rm max}$, we ran a case with and without star formation and used a conservatively low temperature floor $T_F = 1.5 \times 10^4$ K. We performed two additional $V_{\rm max} = 53\,{\rm km\,s^{-1}}$ simulations with a "warm" and "hot" temperature floors at $T_F = 3$ and 5×10^4 K, respectively, and simulated a second $V_{\rm max} = 41\,{\rm km\,s^{-1}}$ case with $T_F = 3 \times 10^4$ K. Higher temperature floors were not explored in the smaller haloes because galaxy formation is suppressed all together if $T_F \sim T_{\rm v}$.[3]

The galaxies were evolved for 5 Gyr, but we find that the global results stabilise after 3 Gyr (see Figure 6 below). The two largest "gas-only" runs without star formation (G74_g and G148_g) produced gas discs that were unstable to their own self-gravity and became clumpy. This is not too surprising given the low T_F adopted, and is consistent with previous claims that substantial heating of the interstellar medium is needed to stabilise disc galaxies (e.g. Robertson et al. 2004). While we have listed radially and vertically average "disc" properties for these unstable cases in Table 1, we do not include these systems in relevant figures below. In order to present results for a large, stable, pure gas disc, we use the $V_{\rm max} = 168\,{\rm km\,s^{-1}}$ simulation from Kaufmann et al. (2007) with $T_F = 3 \times 10^4$ K. This system had a slightly larger spin parameter than the rest of our runs ($\lambda_g = 0.038$).

We note that our final galaxies have larger maximum circular velocity scales than their initial haloes because of the effects of baryonic contraction (compare the second and last columns in Table 1). For example, our D41 series produces galaxies that are comparable in rotation speed to dwarf irregular galaxies like the Large Magellanic Clouds at $\sim 60\,{\rm km\,s^{-1}}$. Our smallest (D24) runs produce galaxies that are large enough ($\sim 35\,{\rm km\,s^{-1}}$) to be included in the Geha et al. (2006) sample of SDSS dwarfs. Our larger galaxies, G74 and G148, produce systems that are comparable to M33 ($\sim 100\,{\rm km\,s^{-1}}$) and the Milky Way ($\sim 200\,{\rm km\,s^{-1}}$).

Finally, we address our initial conditions in light of the idea of "cold flows" put forward by Kereš et al. (2005) and Birnboim & Dekel (2003). These authors find that gas is not shock-heated to the virial temperature in small haloes $M_{\rm v} \lesssim 10^{11} M_\odot$, but rather is accreted as "cold" material, with $T_g \lesssim 10^5$ K. Our models are not strongly at odds with this picture. Specifically, the gas within our small haloes cools very quickly to the temperature floor and indeed falls into the central region in its "cold" phase.

[3] Of course, in a more complicated scenario, feedback from star formation may be the source of the a high effective gas temperature, in which case a dwarf galaxy could form, and subsequently lose its gas once it is heated to $T_g \sim T_{\rm v}$ (see Stinson et al. 2007).

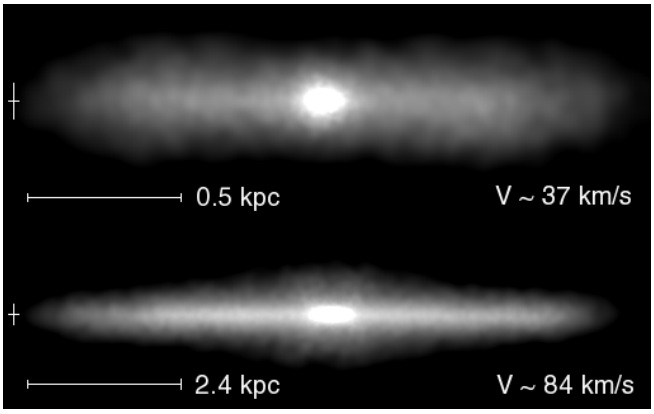

Figure 2. Edge-on views of a simulated dwarf galaxy (D24, upper) and a more massive galaxy (D53, lower). The gray-scale maps the projected stellar density. The disc of the larger galaxy is clearly thinner than the disc of the dwarf. The vertical bars indicate twice the softening length used in the simulations.

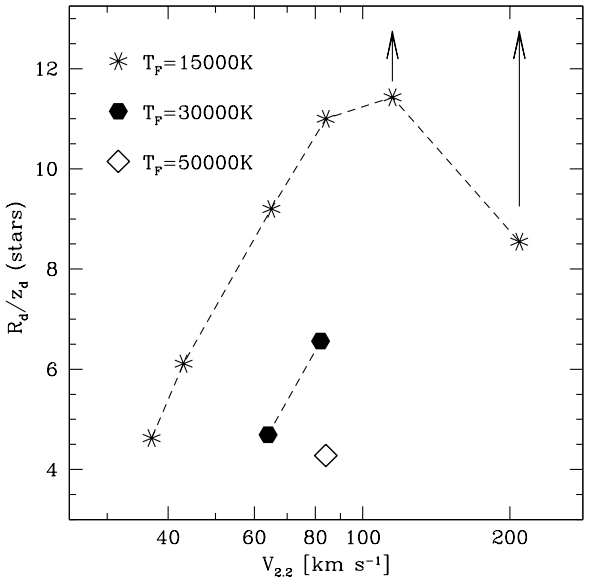

Figure 3. Galaxy disc "thinness" as a function of circular velocity for our star formation runs. Here $V_{2.2}$ is the rotational velocity of the gas measured at $2.2R_{\rm d}$ for each disc. Symbol types correspond to different temperature floors as indicated. Discs are thicker in smaller haloes and for larger temperature floors. The arrows indicate that the stars in the largest galaxies have been artificially thickened by numerical heating.

3.2 Results 1: morphological trends

The upper and lower panels of Figure 2 illustrate the final projected stellar density for the D24 and D53 runs. It is evident that even the mild temperature floor, $T_{\rm F} = 1.5 \times 10^4$ K has resulted in a very thick disc for the small, $\sim 35\,{\rm km\,s^{-1}}$ galaxy, while the larger system, $\sim 85\,{\rm km\,s^{-1}}$, is closer to a standard thin disc.

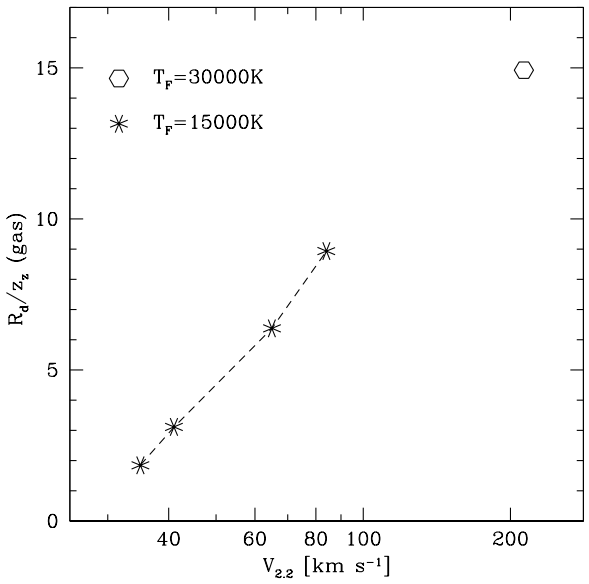

Figure 4. The disc "thinness" as a function of galaxy rotational velocity at $2.2\,R_d$ for our pure gas runs. Symbol types correspond to different temperature floors as indicated. The morphological trend is quite similar to that obtained for our runs with star formation (Figure 3).

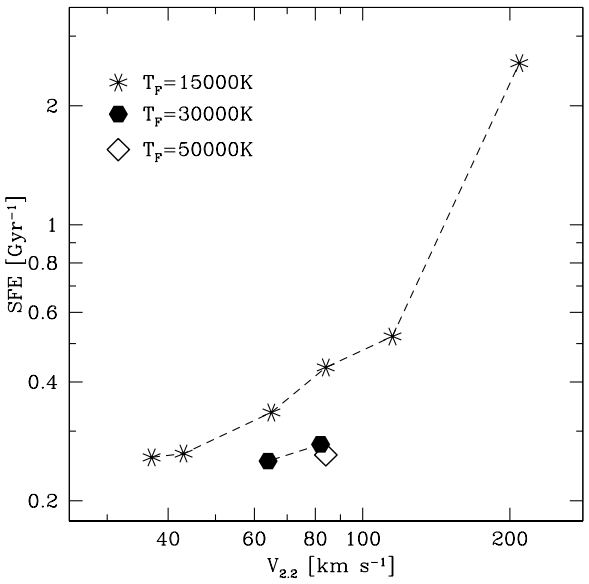

Figure 5. Star formation efficiency (see text) as a function of the galaxy rotational velocity. Symbol types correspond to different temperature floors as indicated.

We note that both of the systems in Figure 2 have formed substantial central bulge components. These central stellar mass concentrations are likely an artifact of our simple initial conditions, which assume a centrally-concentrated NFW profile for the hot gas. We return to this potential shortcoming in §4.

In order to provide a more quantitative comparison between runs, we have estimated a disc scale length, $R_{\rm d}$, and scale height $z_{\rm d}$, for each galaxy. We have explored several methods for quantifying $R_{\rm d}$ and $z_{\rm d}$ and find that our overall results change very little between methods. Because of the large bulge component, our galaxies are not well described by a single exponential surface density profile. Instead of adopting a degenerate two-component fit, we define $R_{\rm d}$ by simply measuring the radius where the face-on stellar (or gas) surface density drops to 0.03 (or $e^{-3.45}$) of its central value, and define this radius to be equal to $3.45R_{\rm d}$. This method is generally insensitive to the details of the functional form of the final disc and probes a radial range that is well sampled with star (or gas) particles. The vertical scale height, $z_{\rm d}$ is determined by fitting an exponential profile to the projected, edge-on surface density profile at a projected radius equal to $R_{\rm d}$ (this avoids the bulge region). The fit is typically good out to vertical scales as large as $z \sim 3\,z_d$ above the disc. The measured values for each simulation are listed in Table 1.

Figure 3 presents the galaxy "thinness" ratio ($R_{\rm d}/z_{\rm d}$) as a function of the (edge-on) *gas* rotational velocity, $V_{2.2}$, measured at $2.2R_{\rm d}$. The points indicated by stars correspond to the $T_{\rm F} = 1.5 \times 10^4$ K cases, while the solid hexagons and open diamond show $T_{\rm F} = 3$ and 5×10^4 K, respectively. It is clear that at a fixed $T_{\rm F}$ small galaxies are naturally thicker than large galaxies. This simple prescription reproduces well the general trend found by Yoachim & Dalcanton (2006) for edge-on galaxy thickness as a function of circular velocity (e.g. their Figure 5).

We note that the two largest galaxies in Figure 3 are artificially thickened (as indicated by the arrows). Both force softening and two-body heating are important in these systems. The force softening acts as an artificial pressure at small scales (Bate & Burkert 1997) and this effect becomes important in the two most massive galaxies G74 and (especially) G148, where the vertical extent of the disc becomes comparable to softening parameter ($f_{\rm res} \simeq 0.25$ and 0.5 kpc, respectively). Furthermore, because the massive galaxies are more efficient in spawning star particles, the ratio of the average star particle mass to dark matter particle mass is higher in the larger galaxies (the ratio is one order of magnitude higher in G148 compared to D24). We therefore expect that our measured z_d values are *over-estimates* of the vertical scale heights compared to what would have been achieved with higher resolution simulations (which would be numerically very expensive). These numerical problems act preferentially to thicken the larger galaxies. Therefore, the general trend with decreasing thickness see between ~ 40 and $100\,{\rm km\,s^{-1}}$ should be robust.

Figure 4 shows that the same morphological trend is seen in our our pure gas runs without star formation. We do not plot the massive G74_g and G143_g galaxies. As mentioned above, the gas became so cold in these runs ($T_F = 1.5{\times}10^4$ K) that the final discs fragmented into thin, clumpy, irregular systems. The open hexagon at $V_{2.2} = 213\,{\rm km\,s^{-1}}$ is simulation G168_gHRLS, where HRLS refers to the Milky Way model described in Kaufmann et al. (2007). This system is hot enough to be stable, with $T_F = 3 \times 10^4$ K, and ends up as very thin disc. Overall, the agreement between our pure gas runs and those with star formation suggests that the correlation between disc thinness and circular velocity should hold, and is largely independent of uncertainties associated with star formation.

3.3 Results 2: gas fractions and star formation

In the previous section we showed that galaxies formed within small haloes tend to be thicker than those formed within large haloes. Figure 5 shows that the star formation efficiency (SFE) in our simulated galaxies also varies as a function of $V_{2.2}$. We define SFE $= \dot{m}_*/m_{\rm g}$, where $\dot{m}_*$ is the star formation rate and $m_{\rm g}$ is the gas associated with the galaxy. Specifically, $m_{\rm g}$ is defined to be the mass of gas that is both cold ($T = T_F$) and no longer infalling. It is evident from Figure 5 that our dwarf galaxies are less efficient in turning gas into stars than are larger galaxies, as expected. Moreover, at fixed circular velocity, the efficiency is reduced for higher ISM temperature floors.

Another observationally-oriented measure of the efficiency of star formation is the cool gas fraction, $m_{\rm g}/(m_{\rm g} + m_*)$. The upper and lower panels of Figure 6 show the evolution of the cool gas with time in our galaxies. We find that the cool gas fraction approaches a constant after ~ 3 Gyr. This corresponds to the time when the infall of new cool gas reaches an equilibrium with the rate that gas is being converted into stars in the galaxy. The upper panel shows the evolution for galaxies with different (final) circular velocities ($V_{2.2}$) at a fixed ISM temperature $T_F = 1.5 \times 10^4$ K. The lower panel shows our D53 series for three values of T_F. Larger systems end up with lower gas fractions, as do systems with decreasing ISM temperatures. Figure 7 shows the same data sliced at a fixed time (3 Gyr) plotted as a function of $V_{2.2}$. Clearly, the gas fractions are higher in smaller galaxies, as expected.

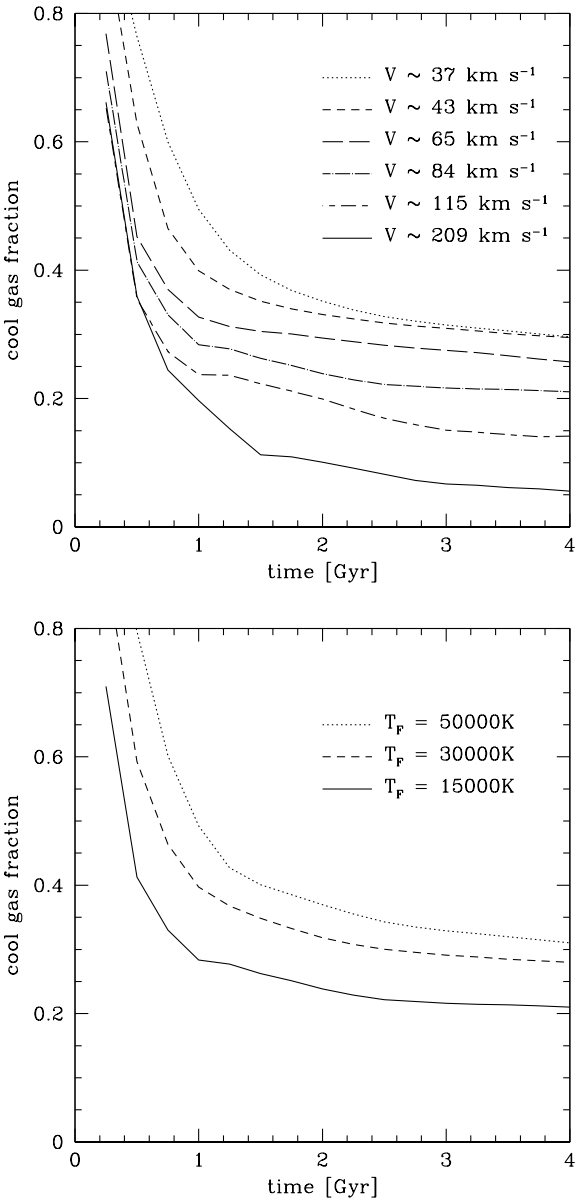

Figure 6. The fraction of cool gas in galaxies as a function of time. The *upper panel* shows runs with different halo masses ($V_{2.2}$ listed) and a fixed ISM temperature floor $T_F = 1.5 \times 10^4$ K. The *lower panel* shows a series of models with the same halo mass (the D53 series) but different T_F values.

4 DISCUSSION

Geha et al. (2006) looked at a sample of 101 extremely low luminosity dwarf galaxies selected from the Sloan Digital Sky Survey, and found a trend for dwarfs to be systematically much more gas rich than giants (e.g. Geha et a. 2006, Figure 3). The results presented in the previous section (Figure 7) show encouraging agreement with the observed trend. However, Geha et al. find an average gas fraction in dwarfs of ~ 0.6, and our simulated dwarfs have gas fractions that are lower ~ 0.3. The comparison may be even worse than it appears because the observations constrain only the neutral H I fraction. At $T \sim 10^4$ K, however, the difference between neutral and total fraction is expected to be small. While we regard the predicted *trend* between gas fraction and velocity scale as the most robust aspect of this work, it is worth investigating whether simple adjustments might bring our results into closer agreement with the data.[4]

An obvious problem with our simulations is that our galaxies all form pronounced bulges (see Figure 2). As discussed elsewhere, the bulges may be artifacts of our simplistic initial conditions, which assume pure NFW profiles for the hot gas haloes (Kaufmann et al., in preparation; see also Hansen & Sommer-Larsen 2006; Mastropietro et al. 2005).

In Figure 8, we have attempted to account for this obvious shortcoming by plotting the *disc* gas fraction as a function of circular velocity for the same set of galaxies shown in Figure 7. Here, we have removed the central stellar component in computing the disc gas fraction, $m_{\rm g}/(m_{\rm g} + m_{*\,\rm disc})$. Specifically, we do not include central stellar material with a spherically-averaged density larger than 2.3×10^9 M$_\odot$ kpc^{-3}, and this eliminates the bulge-like nuclear structures in our galaxies. As seen by the stars, hexagons, and open diamond in Figure 8, these "disc" gas fractions are more in line with observations.

Of course, another clear uncertainty in any galaxy formation simulation is star formation. The most important

[4] Note, however, that these observations possibly underestimate the stellar masses because contributions from extended, low surface brightness stellar populations are likely to be missed (M. Blanton, private communication; or see Roberts & Haynes 1994; van Zee 2001).

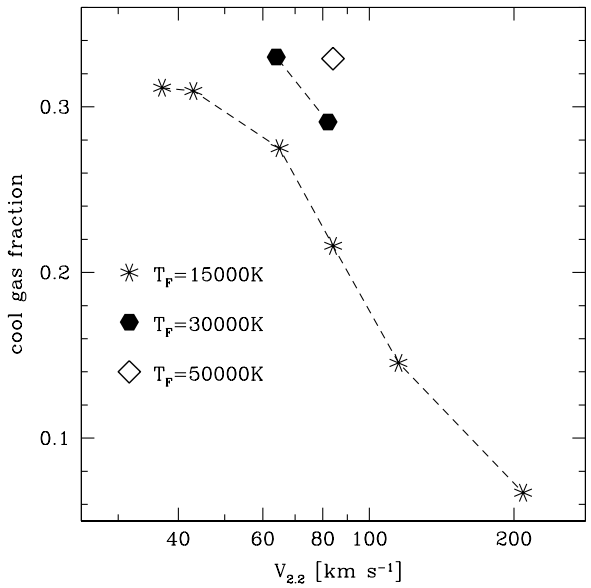

Figure 7. The fraction of cool gas in galaxies as a function of circular velocity. Symbol types correspond to different temperature floors as indicated.

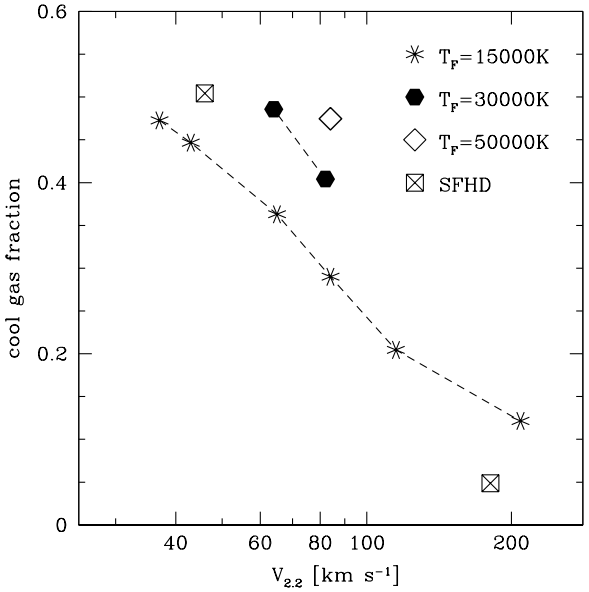

Figure 8. Stars, hexagons, and open diamond show the cool gas fraction in the *disc* for the fiducial series of simulated galaxies (bulge stars have been removed from this measurement, see text for details). As before, the symbol types indicate the temperature floor assumed. The *crossed squares* show the galaxy gas fraction in runs with an increased star formation density threshold $\rho_{\rm SF} \rightarrow 100\rho_{\rm SF}$. For those runs the bulge stars have been included in the measurements.

parameter in our prescription is the density threshold for star formation, $\rho_{\rm SF}$. Observationally, we can constrain only the relationship between the projected gas density and star formation rate (Kennicutt 1998), however, because the density threshold in our prescription is three-dimensional, we are left with the freedom to explore its parameter space.[5] The squares with crosses in Figure 8 show the result of two runs (D24_d and G148_d) with $\rho_{\rm SF}$ set at 100 times our fiducial value (to 2.5×10^8 M$_\odot$ kpc^{-3}). Note that in order to more directly compare with the fiducial runs, we have not excluded bulge stars in these points. As might be expected, the increased threshold produced a much higher gas fraction for the dwarf galaxy compared to the standard case (Figure 7). It also produced a smaller disc than the fiducial run, but a similar axis ratio. Unlike the small galaxy, the gas fraction in the G148_d system is quite similar to that in the fiducial run (Figure 7) because the gas was able to become quite dense and form stars. Like the fiducial Milky Way-size galaxy, this system also sits on the Kennicutt relation. We note, however, that unlike the fiducial case, G148_d produced ~ 10 very dense star clusters in the final disc. Numerical scattering off of these clusters dramatically affected the star particle orbits, and artificially increased the scale height of the final disc.

Elmegreen & Parravano (1994), Blitz & Rosolowski (2004, 2006) and Wong & Blitz (2002) pointed out the relation between the gas pressure in the midplane of the galaxy and the ratio of H_2 versus H I, and related also the star formation efficiency. The gas pressure in the midplane P/k_B in our simulations has values ranging from 4×10^4 to 8×10^5 cm^{-3} K in agreement with the findings of Blitz & Rosolowski (2006), but does not show a strong evolution with galaxy mass. In the simulations the pressure stabilises the gas well above the midplane for the dwarfs, but not for the more massive galaxies, making the midplane pressure less meaningful for the dwarf galaxies.

While it is not the aim of this paper to reproduce the observations in detail, we conclude that there are several physically plausible effects that can eventually lead to a more complete understanding of the gas fractions in small systems. Overall, the agreement between the predicted and observed *trends* is quite encouraging.

5 SUMMARY AND CONCLUSIONS

We have used SPH simulations and an analytic discussion to argue that many of the observed changes in galaxy properties as a function of their rotation speed arise naturally because of the increased importance of ISM pressure in small haloes. Our main results may be summarised as follows:

- An effective ISM temperature floor at $\sim 10^4$ K produces a pressure support radius that is comparable to the angular momentum support radius in dwarf galaxies, $\sim 40\,{\rm km\,s^{-1}}$. This suggests that most small galaxies are not formed as thin discs, but rather are born as thick, puffy systems.
- For a constant temperature floor, pressure support becomes less important in large haloes, and this naturally produces a tendency for massive, isolated galaxies to have thinner discs than their less massive counterparts, as observed.
- The morphological trend produces related trends in star formation efficiency: dwarf galaxies are predicted to have longer star formation time scales than larger galaxies. Simi-

[5] We refer the reader to Kravtsov (2003) for an interesting theoretical discussion on the origin of the Schmidt-Kennicutt relation.

larly, galaxy gas fractions decrease with circular velocity, as observed.

The expected morphological trend seems to be fairly independent of star formation details (compare Figures 3 and 4). While relations of this kind are difficult to quantify observationally for a large number of galaxies, Yoachim & Dalcanton (2006) used a sample of 34 late-type, edge-on, undisturbed disc galaxies to show that more massive galaxies are generally thinner than less massive galaxies (see their Figure 5). They find radial to vertical axis-ratios for dwarf galaxies as low as ~ 3, in agreement with results presented in our Figure 3.

More clues to the nature of galaxy formation on small scales can be gained from the population of dwarf spheroidal galaxies (dSphs). Unlike equally-faint dwarf irregular galaxies (dI), dSphs are gas poor. The fact that gas-poor dwarfs are exclusively found in the proximity of a luminous neighbor (Geha et al. 2006) encourages the notion that tidal forces and ram pressure stripping act to transform dI type galaxies into dSphs (Gunn & Gott 1972; Lin & Faber 1983; Moore & Davis 1994; Mastropietro et al. 2005; Mayer et al. 2001a, 2001b, 2002, 2006, 2007). Typically, models aimed at testing this transformation hypothesis initialise a *thin disc* within a small dark matter halo and investigate how tides or ram-pressure affect the galaxy as it falls into a larger host.

Mayer et al. (2006, 2007) used Smoothed Particle Hydrodynamics (SPH) simulations to show that the combined effects of tides and ram pressure can convert discy dwarfs to gas-poor spheroidal systems, but only if a heating source is imposed to keep the gas in the dwarf extended and hot at a temperature of $\sim 2.5 \times 10^4$K (L. Mayer, private communication). As we have shown, temperature floors of this magnitude inhibit the formation of thin discy dwarfs in the field. If a puffy dwarf of the kind we expect falls into the potential well of a larger galaxy with an extended hot gas halo, it should be quite susceptible to gas loss and morphological transformation. Trends of this kind do seem to be broadly in accord with some observations (e.g. Lisker et al. 2007, Geha et al. 2006). In another investigation, Mastropietro et al. (2005) used N-body simulations to study the transformation of discy dwarfs to spheroidal dwarfs. They had some success, but were unable to reproduce the observed fraction of spheroidal dwarfs with negligible rotational support. Our results suggest that field dwarfs are likely to be born thicker than typically assumed and are therefore more susceptible to kinematic transformations.

It has long been recognised that galaxy formation must become increasingly inefficient in dark matter haloes from the scale of big spirals to small dwarfs (White & Reese 1978; Klypin et al. 1999; Moore et al. 1999; Strigari et al. 2007). Our work suggests that it is difficult to avoid the suppression of galaxy formation efficiency in small haloes. Shallow potential wells naturally give rise to puffy galaxies with long star formation time scales. This situation makes them more susceptible to other feedback effects and external influences that may act to suppress star formation even further. Small galaxies are also systematically more metal poor than larger systems (e.g. Tremonti et al. 2004). The lower efficiency of star formation may also explain the observed mass-metallicity relation without the need for strong winds (Tassis et al. 2006). For example, Brooks et al. (2007) recovered in their cosmological simulations the observed relation only by including an allowance for ISM heating (see also Ricotti & Gnedin 2005).

A natural extension of this work would be a more detailed modeling of the coupling between various energy sources and the ISM. Ideally, this would include a star formation prescription based on molecular cooling and radiative transfer for the treatment of the feedback from stars to the ISM - allowing to overcome the simple proxy of a temperature floor.

ACKNOWLEDGMENTS

It is a pleasure to thank James Wadsley, Joachim Stadel and Tom Quinn for making GASOLINE available to us. The numerical simulations were performed on the zBox2 supercomputer at the University of Zürich (`http://www.zbox2.org`) and the IA64 Linux cluster at the San Diego Supercomputer Center. We thank Doug Potter, Joachim Stadel and Ben Moore for building the zBox2 and allowing us to run parts of the simulations on it. We would like to thank Stelios Kazantzidis for providing a code to generate isolated dark matter haloes. We acknowledge useful and stimulating discussions with Michael Blanton, Julianne Dalcanton, Marla Geha, Andrey Kravtsov, Ariyeh Maller, Lucio Mayer, Brant Robertson, Greg Stinson, Liese van Zee, Betsy Barton and Louis Strigari. We also thank the anonymous referee for valuable comments. This work was supported by the Center for Cosmology at UC Irvine.

REFERENCES

Balsara, D. S. 1995, Journal of Computational Physics, 121, 357
Barnes, J., & Efstathiou, G. 1987, ApJ, 319, 575
Bate, M. R., & Burkert, A. 1997, MNRAS, 288, 1060
Benson, A. J., Lacey, C. G., Baugh, C. M., Cole, S., & Frenk, C. S. 2002, MNRAS, 333, 156
Birnboim, Y., & Dekel, A. 2003, MNRAS, 345, 349
Blitz, L., & Rosolowsky, E., 2004, ApJ, 612, L29
Blitz, L., & Rosolowsky, E., 2006, ApJ, 650, 933
Blumenthal, G., Faber, S. & Primack, J. 1986, ApJ, 301, 27
Brinchmann, J., Charlot, S., White, S. D. M., Tremonti, C., Kauffmann, G., Heckman, T., & Brinkmann, J., 2004, MNRAS, 351, 1151
Brooks, A. M., Governato, F., Booth, C. M., Willman, B., Gardner, J. P., Wadsley, J., Stinson, G., & Quinn, T. 2007, ApJ, 655, L17
Bullock, J. S., Kravtsov, A. V., & Weinberg, D. H. 2000, ApJ, 539, 517
Bullock, J. S., Kolatt, T. S., Sigad, Y., Somerville, R. S., Kravtsov, A. V., Klypin, A. A., Primack, J. R., & Dekel, A. 2001a, MNRAS, 321, 559
Bullock, J. S., Dekel, A., Kolatt, T. S., Kravtsov, A. V., Klypin, A. A., Porciani, C., & Primack, J. R., 2001b, ApJ, 555, 240
Crain, R. A., Eke, V. R., Frenk, C. S., Jenkins, A., McCarthy, I. G., Navarro, J. F., & Pearce, F. R., 2007, MNRAS, 377, 41

Dalcanton, J. J., Yoachim, P., & Bernstein, R. A., 2004, ApJ, 608, 189
Dekel, A., & Woo, J.2003, MNRAS, 344, 1131
Dekel, A., & Silk, J. 1986, ApJ, 303, 39
Dutton, A. A., van den Bosch, F. C., Dekel, A., & Courteau, S. 2007, ApJ, 654, 27
Efstathiou, G. 1992, MNRAS, 256, 43P
Fall, S. M. & Efstathiou, G. 1980, MNRAS, 193, 189
Geha, M., Blanton, M. R., Masjedi, M., & West, A. A. 2006, ApJ, 653, 240
Gnedin, N. Y. 2000, ApJ, 542, 535
Gnedin, O. Y., Weinberg, D. H., Pizagno, J., Prada, F., & Rix, H.-W. 2006, ArXiv Astrophysics e-prints, arXiv:astro-ph/0607394
Gunn, J. E., & Gott, J. R. I. 1972, ApJ, 176, 1
Hansen, S. H., & Sommer-Larsen, J. 2006, ApJ, 653, L17
Hoeft, M., Yepes, G., Gottlöber, S., & Springel, V., 2006, MNRAS, 371, 401
Hunter, D. A., & Gallagher, J. S., III 1985, ApJS, 58, 533
Kauffmann, G., White, S. D. M., & Guiderdoni, B. 1993, MNRAS, 264, 201
Kauffmann, G., et al. 2003, MNRAS, 341, 54
Kaufmann, T., Mayer, L., Wadsley, J., Stadel, J., & Moore, B. 2007, MNRAS, 375, 53
Katz, N. 1992, ApJ, 391, 502
Kazantzidis, S., Magorrian, J., & Moore, B., 2004, ApJ, 601, 37
Kennicutt, R. C., Jr., 1998, ApJ, 498, 541
Kereš, D., Katz, N., Weinberg, D. H., & Davé, R., 2005, MNRAS, 363, 2
Klypin, A., Kravtsov, A. V., Valenzuela, O., & Prada, F. 1999, ApJ, 522, 82
Kravtsov, A. V. 2003, ApJ, 590, L1
Kravtsov, A. V., Gnedin, O. Y., & Klypin, A. A. 2004, ApJ, 609, 482
Lin, D. N. C., & Faber, S. M. 1983, ApJ, 266, L21
Lisker, T., Grebel, E. K., Binggeli, B., & Glatt, K., 2007, ArXiv Astrophysics e-prints, arXiv:astro-ph/0701429
Macciò, A. V., Dutton, A. A., van den Bosch, F. C., Moore, B., Potter, D., & Stadel, J. 2006, ArXiv Astrophysics e-prints, arXiv:astro-ph/0608157
Maller, A. H. & Bullock, J. S. 2004 MNRAS, 355, 694
Mastropietro, C., Moore, B., Mayer, L., Debattista, V. P., Piffaretti, R., & Stadel, J., 2005, MNRAS, 364, 607
Mayer, L., Governato, F., Colpi, M., Moore, B., Quinn, T., Wadsley, J., Stadel, J., & Lake, G. 2001a, ApJ, 559, 754
Mayer, L., Governato, F., Colpi, M., Moore, B., Quinn, T., Wadsley, J., Stadel, J., & Lake, G., 2001b, ApJ, 547, L123
Mayer, L., Moore, B., Quinn, T., Governato, F., & Stadel, J. 2002, MNRAS, 336, 119
Mayer, L., Mastropietro, C., Wadsley, J., Stadel, J., & Moore, B. 2006, MNRAS, 369, 1021
Mayer, L., Kazantzidis, S., Mastropietro, C., & Wadsley, J., 2007, Nature 445, 738
McKee, C. F., & Ostriker, J. P., 1977, ApJ, 218, 148
Mo, H. J., Mao, S. & White, S., 1998, MNRAS, 295, 319
Monaghan, J. J. 1992, ARAA, 30, 543
Moore, B., & Davis, M. 1994, MNRAS, 270, 209
Moore, B., Ghigna, S., Governato, F., Lake, G., Quinn, T., Stadel, J., & Tozzi, P. 1999, ApJ, 524, L19
Navarro, J. F., Frenk, C. S., & White, S. D. M., 1996, ApJ, 462, 563
Elmegreen, B. G., & Parravano, A., 1994, ApJ, 435, L121
Peebles, P. J. E. 1969, ApJ, 155, 393
Quinn, T., Katz, N., & Efstathiou, G. 1996, MNRAS, 278, L49
Read, J. I., Pontzen, A. P., & Viel, M., 2006, MNRAS, 371, 885
Ricotti, M., & Gnedin, N. Y., 2005, ApJ, 629, 259
Roberts, M. S., & Haynes, M. P., 1994, ARA&A, 32, 115
Robertson, B., Yoshida, N., Springel, V., & Hernquist, L. 2004, ApJ, 606, 32
Robertson, B., Bullock, J. S., Cox, T. J., Di Matteo, T., Hernquist, L., Springel, V., & Yoshida, N. 2006, ApJ, 645, 986
Somerville, R. S., & Primack, J. R. 1999, MNRAS, 310, 1087
Somerville, R. S. 2002, ApJ, 572, L23
Springel, V., & Hernquist, L., 2003, MNRAS, 339, 289
Stadel J., 2001, PhD Thesis, U. Washington
Stinson, G., Seth, A., Katz, N., Wadsley, J., Governato, F., & Quinn, T. 2006, MNRAS, 373, 1074
Stinson, G. S, Dalcanton, J. J., Quinn, T., Kaufmann, T., & Wadsley, J., 2007, ApJ accepted, ArXiv e-prints, arXiv:0705.4494
Strigari, L. E., Bullock, J. S., Kaplinghat, M., Diemand, J., Kuhlen, M., & Madau, P. 2007, ArXiv e-prints, arXiv:0704.1817
Tassis, K., Kravtsov, A. V., & Gnedin, N. Y. 2006, ArXiv e-prints, arXiv:astro-ph/0609763
Taylor, E. N., & Webster, R. L., 2005, ApJ, 634, 1067
Thoul, A. A., & Weinberg, D. H. 1996, ApJ, 465, 608
Tremonti, C. A., et al. 2004, ApJ, 613, 898
van Zee, L. 2001, AJ, 121, 2003
Wadsley J., Stadel J., Quinn T., 2004, NewA, 9, 137
White, S. D. M., & Frenk, C. S. 1991, ApJ, 379, 52
White, S. D. M., & Rees, M. J., 1978, MNRAS, 183, 341
Wong, T., & Blitz, L. 2002, ApJ, 569, 157
Yepes, G., Kates, R., Khokhlov, A., & Klypin, A. 1997, MNRAS, 284, 235
Yoachim, P., & Dalcanton, J. J. 2006, AJ, 131, 226